UNIVERSITY OF TARTU

FACULTY OF SCIENCE AND TECHNOLOGY

Institute of Physics

Kaarel Kaldvee

THE INFLUENCE OF LASER EXCITATION WAVELENGTH ON THE HEATING OF THE NEODYMIUM DOPED FLUORIDE NANOPARTICLES AS THE RESULT OF THE MULTIPHONON RELAXATION

Bachelor's thesis (12 ECTS)

Supervisor: Dr. hab., Ph.D. Yury Orlovskiy

Allowed for defense …….

Supervisor ……....

Tartu 2015

Contents

List of abbreviations 3

1 Introduction 4

2 Overview of the field 5

2.1 Temperature effect on emission spectra 5

2.2 Multiphonon relaxation 5

2.3 The requirements for the nanoparticles 6

3 Material and methods 7

3.1 The LaF_3 nanocrystals doped with Nd^{3+} ions 7

3.2 Experiment setup 8

3.3 The experimental 9

4 Results and analysis 10

4.1 The spectrum and energy levels 10

4.2 Fluorescence kinetics 13

4.3 Comparison of spectra from two different cryosystems 13

4.4 Different excitation wavelengths 15

4.5 Temperature dependence 18

5 Summary 22

6 Acknowledgements 22

7 Mitmefoononilise relaksatsiooni mõju neodüümiga dopeeritud fluoriidi nanoosakeste soojendamisele timmitaval laserergastusel 24

8 References 24

List of abbreviations

RE	rare-earth
NP	nanoparticle
MR	multiphonon relaxation
TEM	transmission electron microscopy
LLS	Laboratory of Laser Spectroscopy
CS	cryosystem
CCR	closed cycle refrigerator
OPO	optical parametric oscillator
PMT	photomultiplier
ICCD	intensified charge-coupled device
PHL	photoluminescence
CF	crystal field
au	arbitrary unit

1 Introduction

Regardless of the huge progress made in the science and medicine, cancer is still among the leading causes of mortality worldwide and the number of new cases is expected to rise by about 70% over the next 20 years [1]. The rare-earth doped nanoparticles (NP) can be used for photo-induced heating for hyperthermia, possibly suitable for local heating of cancer cells for noninvasive treatment. The idea is to heat the rare-earth doped nanoparticles in the process of multiphonon relaxation of the optical excitation energy [2].

A good candidate as the dopant is Nd^{3+} ion. It has a high absorption cross-section in the transparency window of biological tissues and could also be used as a biomarker [3]. The LaF_3 crystal matrix with a maximal phonon energy $\hbar\omega_{max.} = 400\ cm^{-1}$ [4] is chosen as the host for Nd^{3+} ions. In this configuration three phonons will bridge the energy gap for the $^2H_{9/2} + {}^4F_{5/2} \rightarrow {}^4F_{3/2}$ transition during the multiphonon relaxation. [4]

The aim of this work is to investigate the influence of laser excitation wavelength on heating of the Nd^{3+}:LaF_3 nanoparticles as the result of multiphonon relaxation. For this the 2 at% Nd^{3+}:LaF_3 nanoparticles were first synthesized and then studied using fluorescence emission spectroscopy. The method to study the dependence of heating of the rare-earth doped nanoparticles on the wavelength of optical excitation is developed. In so doing, both He-bath cryostat and closed cycle refrigerator, with a cold finger inside the vacuum chamber, were used to cool the powder of the 2 at% Nd^{3+}:LaF_3 nanocrystals down to 10 K and the fluorescence spectra of the $^4F_{3/2} \rightarrow {}^4I_{9/2}$ transition were measured under laser pulses of optical parametric oscillator at 522, 577.5 and 789 nm excitation wavelengths (respectively into the $^4G_{7/2}$, $^4G_{5/2}$ and $^2H_{9/2}$+ $^4F_{5/2}$ level). Then the temperature was gradually increased up to 175 K while measuring fluorescent spectra at different temperatures. Also different time gates were used while measuring the fluorescence spectra. As the last part of the work the data was collected, processed and analyzed.

All parts of this work other than the synthesis of the nanocrystals and TEM imaging were done by the author with the instructions from the supervisor.

2 Overview of the field

2.1 Temperature effect on emission spectra

The zero-phonon line and the phonon sideband constitute the line shape of individual light emitting molecule doped into a solid matrix. A phonon is a quantized mode of vibration occurring in a rigid crystal lattice. When the matrix contains many fluorophores, each of them contribute a zero-phonon line and a phonon sideband to the emission spectra. The emission spectra originating from a collection of identical fluorophores in a matrix is said to be inhomogeneously broadened, because each fluorophore is surrounded and modified by a slightly different matrix environment. The difference in intensity between the zero-phonon line and the phonon sideband strongly depends on the temperature. However, in the RE (except for Yb^{3+}) ions doped crystals due to super-weak electron-phonon coupling the phonon sidebands are extremely weak comparing to zero-phonon lines [5]. At very low temperatures (near absolute zero) the zero-phonon lines can become extremely narrow and the effect of inhomogeneous broadening is well pronounced [6].

2.2 Multiphonon relaxation

Rare-earth (RE) ions commonly present a rich energy level diagram and doping them into dielectric materials leads to the presence of energy levels in the band gap. In cancer treatment research the rare-earth doped nanoparticles are studied mainly for possible application in bioimaging the cancer tumor. Another prospect could be photo-induced local heating of the cancer cells for hyperthermia. [4, 7]

The idea of heating nanoparticles is centered on the process of multiphonon relaxation (MR) of the optical excitation energy in the rare-earth doped crystals. The MR actually is a negative effect to fluorescent properties of materials because it competes with radiative relaxation, but it can be used as a positive effect for nanoscale heaters. [2]

In the single frequency model of lattice vibrations the rate of multiphonon relaxation is raised by one or two orders of magnitude just by a decrease of phonon number p by one bridging the energy gap ΔE

$$p = \frac{\Delta E}{\hbar\omega_{eff}} ,$$

where ΔE is the energy gap between two electronic levels and $\hbar\omega_{\mathrm{eff}}$ stands for effective phonon energy in single frequency model of lattice vibrations. If phonon number is equal or less than three, then the MR almost completely dominates the fluorescence, because the rate of multiphonon transition is on the nanosecond or picosecond time scale while the spontaneous emission rates is 10^5 – 10^7 times slower for the rare-earth ions. [2]

2.3 The requirements for the nanoparticles

The biomedical application sets strict requirements for the nanoparticles. They must absorb in the transparency window of biological tissue (750 – 1300 nm) and if used for bioimaging, also emit in that region. The NPs need to be water dispersible, since the internal media of human organism is aqueous. The size of the particles has to be less than 100 nm in diameter and have a narrow size distribution to have high cellular uptake. They also need to be nontoxic and have high crystallinity. [8]

The Nd^{3+}:LaF_3 particles, which normally are studied for bioimaging application, are reported to be biocompatible, but the size of the particles and the water dispersibility is strongly dependent on method of the synthesis. One method to synthesize suitable particles is to use the microwave-hydrothermal technique described in Refs. [3, 8]. The Nd^{3+} ion qualifies for both hyperthermia and bioimaging. It can be excited at the beginning of near-infrared region into the $^2H_{9/2}$ + $^4F_{5/2}$ level (~790 nm) and has three emission bands in the transparency window of biological tissue, the $^4F_{3/2} \rightarrow {}^4I_{9/2}$, $^4F_{3/2} \rightarrow {}^4I_{11/2}$, and $^4F_{3/2} \rightarrow {}^4I_{13/2}$ transitions. [9]

3 Material and methods

3.1 The LaF_3 nanocrystals doped with Nd^{3+} ions

For the synthesis of the 2 at% Nd^{3+}:LaF_3 nanoparticles solutions of $La(NO_3)_3 \cdot 6H_2O$ and $Nd(NO_3)_3 \cdot 5H_2O$ were prepared in 10 ml of deionized water, as well as the solution of NH_4F in 30 ml of deionized water. After that the solutions of nitrates were added dropwise to the solution of fluoride under vigorous stirring and left under stirring for 15 min. The freshly precipitated gel was diluted in the mother solution with 10 ml of deionized water. In order to increase the dispersibility of the resulting nanoparticles the sodium citrate tribasic dehydrate was added to the rare-earth nitrates solution mixture before the gel precipitation.

Then the gel was transferred into the 100 ml Teflon autoclave and exposed to microwave-hydrothermal treatment (200 ^{o}C, 4 hours) using Berghof Speedwave-4 laboratory device (2.45 GHz, 1 kW maximum output power). After the treatment the sample was centrifuged, washed several times with deionized water and air-dried at 100 ^{o}C for 2 hours.

The size and shape of synthesized 2 at% Nd^{3+}:LaF_3 nanoparticles were characterized with transmission electron microscopy (TEM) (Figure 1). The size of nanoparticles is within the range of 20 and 50 nm.

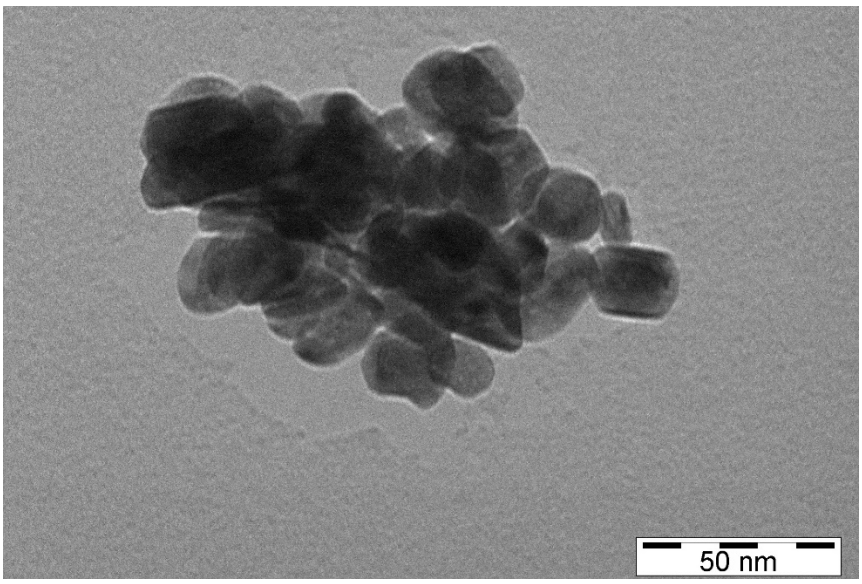

Figure 1. TEM picture of aggregated Nd^{3+}:LaF_3 nanoparticles. The particles are mostly in the size of 30-40 nm.

3.2 Experiment setup

The experiment was conducted in Laboratory of Laser Spectroscopy (LSS) in Institute of Physics. Two different setups, which differ the most in the method of cooling the sample, were used to measure the spectra. One method used helium bath and the other cold finger in the vacuum cryostats to refrigerate the sample. In both cases the pulsed laser excitation of the optical parametric oscillator (OPO) Ekspla NT342/1/UVE (t_p = 15 ns, f = 20 Hz) was used.

In case of helium bath method the UTREKS-LSO cryosystem (CS) was used (Figure 2). The sample is cooled by helium vapors and the temperature is determined by controlling the flow of gas and by the heater. The long-pass filter BLP-785R (Semrock) was attached before the front slit of the monochromator to block the scattered light of laser excitation. The fluorescence was dispersed by the MDR-23 LOMO monochromator and detected by the photomultiplier (PMT) Pheu-79 in the photon counting mode using LabJack U6 data acquisition unit (for spectra) or multi-channel analyzer MCA Series/P7882 (for fluorescence kinetics) with 100 ns time resolution.

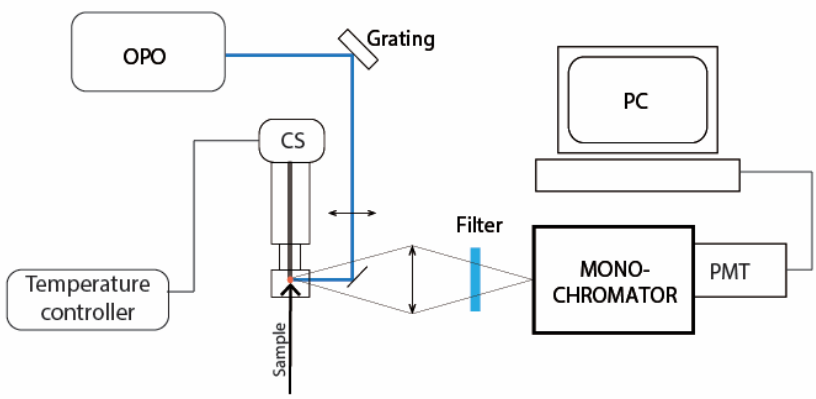

Figure 2. Scheme of using the helium bath cryosystem and PMT.

In the other case Janis closed cycle refrigerator (CCR) system was used (Figure 3). CCR system does not require liquid helium as a source of cooling. Helium gas is compressed and expanded in a closed loop and during each expansion phase, heat is removed from the cold finger and the sample mounted on it, which are located in a vacuum chamber. A heater and thermometer installed on the cold finger are used to control the sample temperature. As this was the first experiment done on Janis CCR in LSS, the capabilities and limitations of the apparatus were not

really well know yet and a lot was learned about the setup, that will be used in future works. The sample was excited by nanosecond laser pulses from OPO and the same long-pass filter BLP-785R was used before spectrograph Andor Shamrock 303i. The fluorescence was detected by Andor iStar intensified charge-coupled device (ICCD).

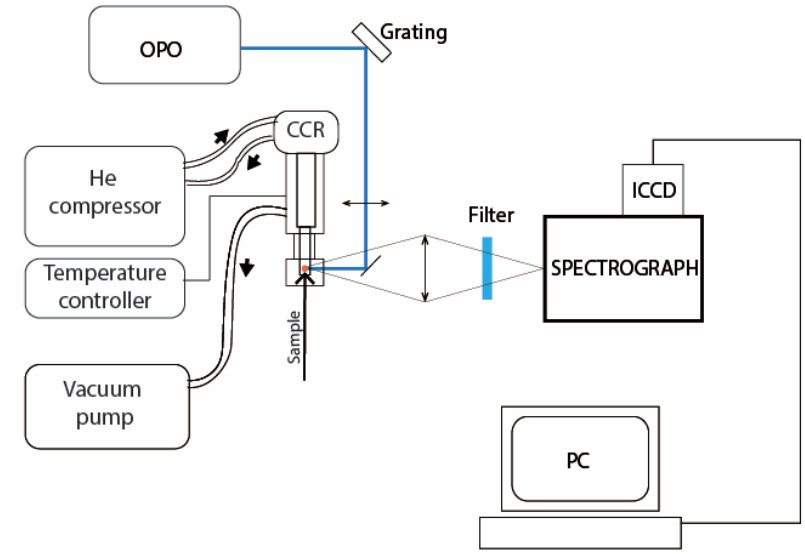

Figure 3. Scheme of the experiment setup with Janis CCR and Andor iStar ICCD.

3.3 The experimental

First the photoluminescence (PHL) spectra of the nanoparticles were measured in helium-bath cryosystem using 577.5 nm laser excitation at 10 K. After that we measured the fluorescence kinetics at different excitation laser wavelengths detected at the most intensive emission spectral line to do site-selective spectroscopy. Then the temperature dependence of the spectral line width was measured at 50 and 100 K.

Next we changed to Janis CCR and cooled the sample down to 10 K. PHL spectra were measured at different excitation wavelengths: 522, 577.5, and 789 nm. For each excitation two different time gates were used. One was with zero delay and 5 μs width (t_D = 0 μs, Δt = 5 μs) just after laser excitation and the other with 200 μs delay and 100 μs width (t_D = 200 μs, Δt = 100 μs).

The temperature dependence of spectra were measured with the step of 10 K till 100 K and then with 25 K step up to 175 K. At all temperatures two different time gates were used: zero delay with 10 μs width (t_D = 0 μs, Δt = 10 μs) and 200 μs delay with 100 μs width (t_D = 200 μs, Δt = 100 μs).

4 Results and analysis

4.1 The spectrum and energy levels

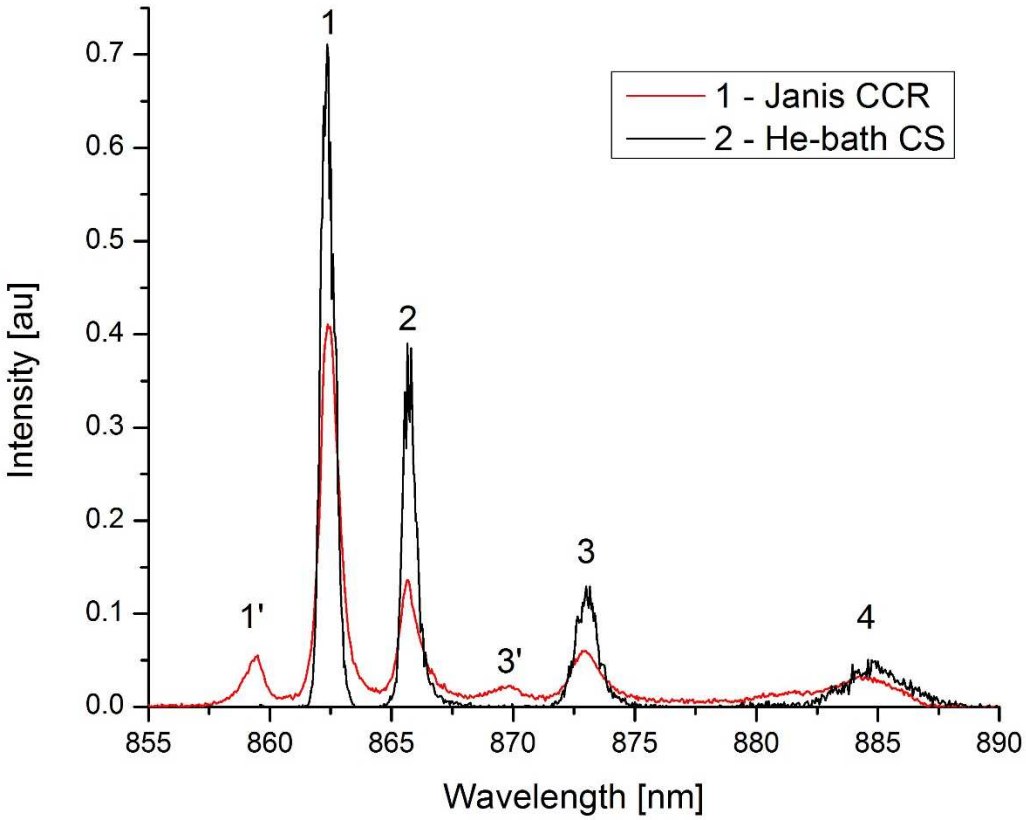

Figure 4. A fluorescence spectrum of 2 at% Nd^{3+}: LaF_3 at 10 K measured with two different setups: He-bath cryostat and cold finger cryostat at 10 K. The same numeration is used in the whole work to identify the spectral lines. The excitation wavelength for curve 1 is 789 nm into the $^2H_{9/2}$ + $^4F_{5/2}$ level and for curve 2 it is 577.5 nm into the $^4G_{5/2}$ level. The heating due to the multiphonon relaxation can be seen on curve 1.

To identify the transitions, the spectrum measured with ICCD and cooled with CCR (Figure 4, curve 1) is compared with the Ref. [4]. Our detector sensitivity drops rapidly before 900 nm, but one optical transition is expected to be around 901 nm, which in our case is not detectable, but is still marked in Table 1 and 2.

In Ref. [4], it is stated that peaks 1' and 3' are not presented at liquid helium temperature and our helium bath experiment confirmed that (Figure 4, curve 2). This indicates that their origin is the optical transitions from the second crystal field (CF) level of the $^4F_{3/2}$ manifold, which is populated at temperatures higher than 10 K. The fact that they are presented on spectrum 1 (Figure 4, curve 1) shows that the temperature of the 2 at% Nd^{3+}: LaF_3 sample is higher than the

temperature of cold finger for Janis CCR setup (10 K). This is caused by multiphonon relaxation from the $^2H_{9/2}$ + $^4F_{5/2}$ level to the $^4F_{3/2}$ metastable level and will be discussed later (chapter 4.4 and 4.3). The spectral lines 1, 2, 3, and 4 (Figure 4) are connected with the $^4F_{3/2}(1) \rightarrow {}^4I_{9/2}$ transitions and can be thereby used to determine the energies for the $^4I_{9/2}$ crystal field levels (Table 1).

Table 1. Crystal field levels for the $^4I_{9/2}$ manifold in the 2 at% Nd^{3+}: LaF_3 nanoparticles.

Level	$^4I_{9/2}(1)$	$^4I_{9/2}(2)$	$^4I_{9/2}(3)$	$^4I_{9/2}(4)$	$^4I_{9/2}(5)$
Energy (cm^{-1})	0	45	99	141	~500

Table 2. Optical transitions in the 2 at% Nd^{3+}: LaF_3 nanoparticles and their energies and wavelengths.

Number	Transition	Energy (cm^{-1})	Difference with reference (cm^{-1})	Wavelength (nm)
1’	$^4F_{3/2}(2) \rightarrow {}^4I_{9/2}$ (1)	11635	-3	859.5
1	$^4F_{3/2}(1) \rightarrow {}^4I_{9/2}$ (1)	11596	+1	862.4
2	$^4F_{3/2}(1) \rightarrow {}^4I_{9/2}$ (2)	11551	+4	865.7
3’	$^4F_{3/2}(2) \rightarrow {}^4I_{9/2}$ (3)	11497	+2	869.8
3	$^4F_{3/2}(1) \rightarrow {}^4I_{9/2}$ (3)	11455	-1	873.0
4	$^4F_{3/2}(1) \rightarrow {}^4I_{9/2}$ (4)	11310	+5	884.2
5*	$^4F_{3/2}(1) \rightarrow {}^4I_{9/2}$ (5)	~11100		~901

*The last line is not visible on the spectrum, because the transition is outside the spectral range of the detector used.

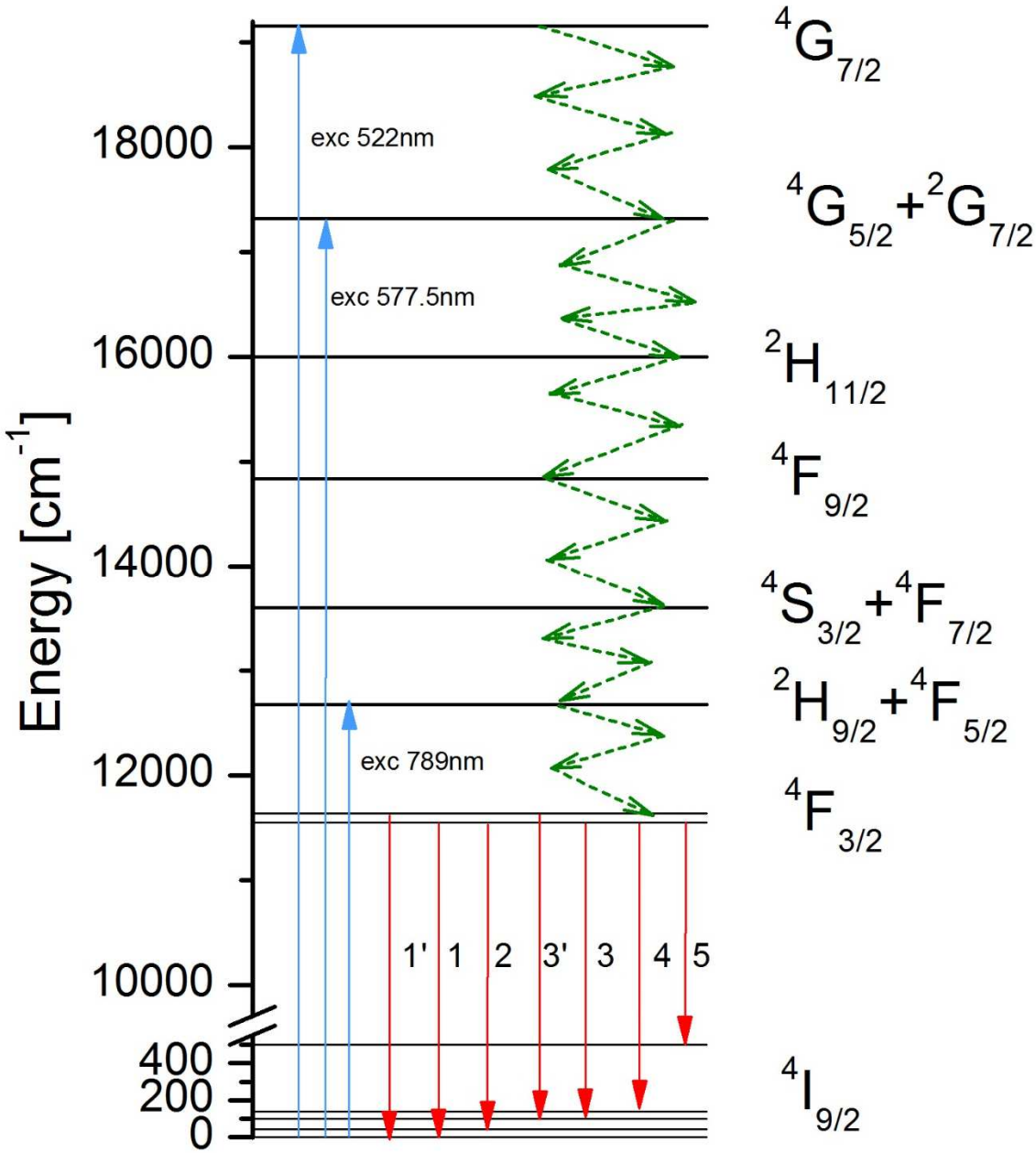

Figure 5. The energy levels for Nd^{3+} in the LaF_3 bulk crystal taken from Ref. [4]. Blue arrows show the excitation wavelengths used and the red arrows show the transitions that are detected in the emission spectrum (Figure 4, curve 1). Green dashed arrows show the multiphonon relaxation process and number of arrows indicates the number of phonons emitted in the transition between the energy levels. Note that the transitions 1' and 3' start from $^4F_{3/2}$(2). The transition $^4F_{3/2}(1) \rightarrow {}^4I_{9/2}$ (5) is outside the spectral range of the detector and is not visible on the spectrum.

Compared Figure 5 with Table 2 a conclusion can be made that the CF levels for bulk Nd^{3+}: LaF_3 crystal and nanocrystals are the same.

4.2 Fluorescence kinetics

To measure the fluorescence decay curves the sample is excited with 577.5 nm into the $^4G_{5/2}$ level and the time dependent spectra are measured at five different wavelengths (862.3, 862.5, 862.8, 863.3 and 863.4 nm) on the main spectral line (the $^4F_{3/2}(1) \rightarrow {}^4I_{9/2}$ (1) transition) with spectral resolution 1.6 cm^{-1} (0.12 nm) (Fig. 6). Although the spontaneous emission lifetimes determined from the slopes of late stages of the curves are close to τ_R = 500 μs, it is clearly visible that the time profiles of the curves at the initial stages are different. Thus we can say that we are dealing with different types of optical centers and the spectral line is inhomogeneously broadened. [5]

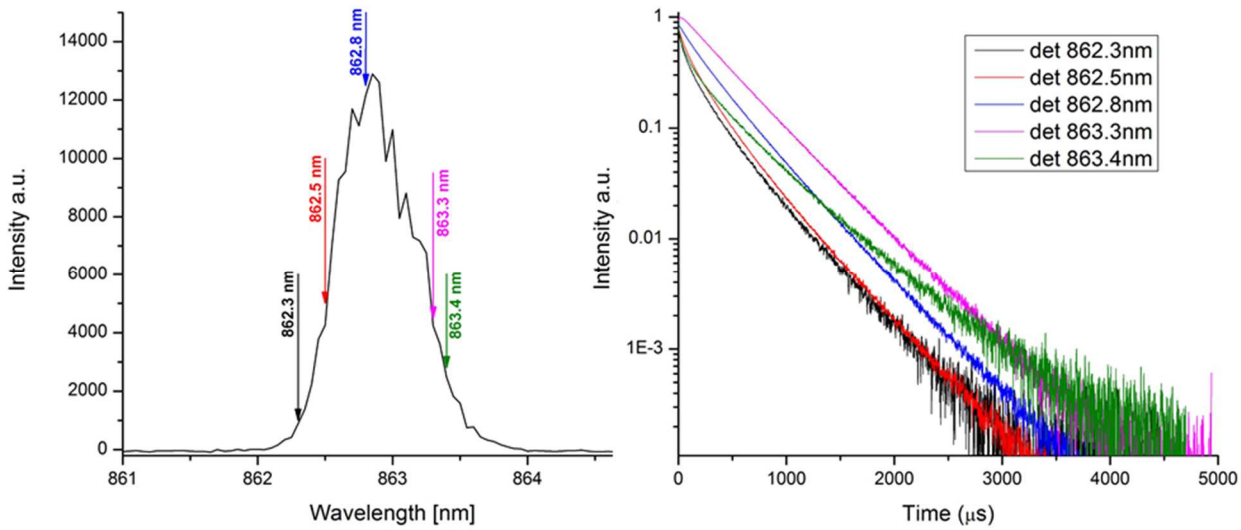

Figure 6. Graph a) shows the spectral line detected at the $^4F_{3/2}(1) \rightarrow {}^4I_{9/2}$ (1) transition in the 2 at% Nd^{3+}:LaF_3 nanoparticles at 10 K in He-bath CS with spectral resolution 1.6 cm^{-1} (0.12 nm) and the detection wavelengths for the fluorescence kinetics; graph b) shows the fluorescence kinetics. A 577.5 nm laser excitation wavelength into the $^4G_{5/2}$ level was used. The decay curves are normalized to the maximal intensity for better comparison.

4.3 Comparison of spectra from two different cryosystems

As already seen (Figure 4) when cooling the sample with Janis CCR the spectrum is not as narrow as in case of cooling with He-bath CS although for both cases the temperature was set to be 10 K. The presence of $^4F_{3/2}(2) \rightarrow {}^4I_{9/2}$ (1) and $^4F_{3/2}(2) \rightarrow {}^4I_{9/2}$ (3) transitions (Figure 4, curve 1) indicates that the actual temperature of the sample in Janis CCR is significantly higher.

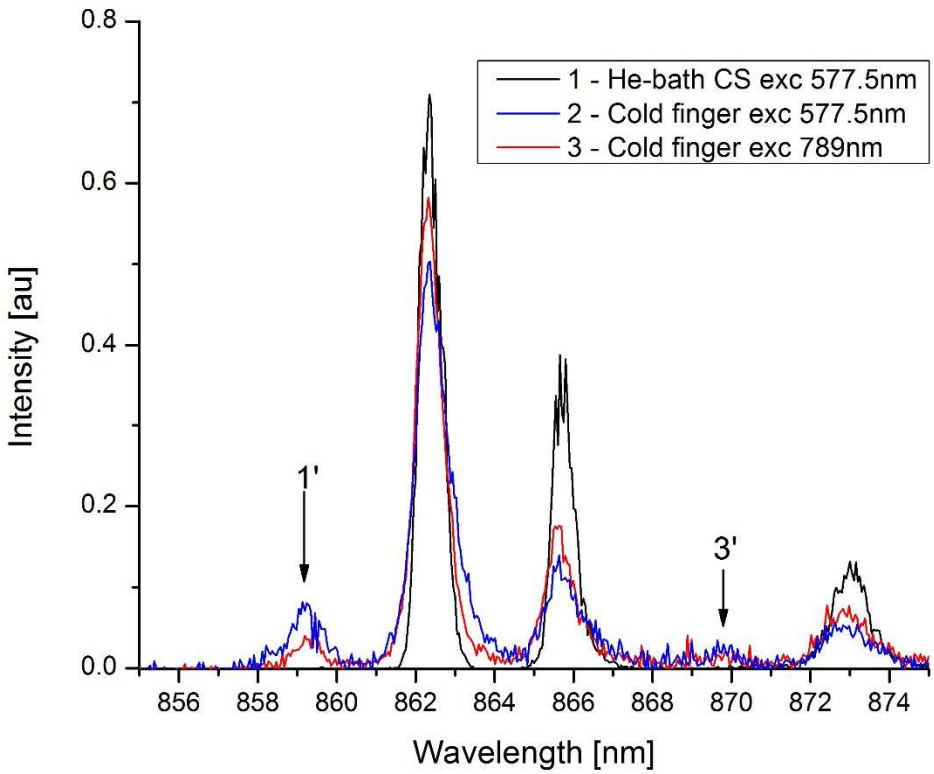

Figure 7. Three fluorescence spectra of 2 at% Nd^{3+}:LaF_3 nanoparticles, normalized to unity area, demonstrates the effect of heating the sample positioned on cold finger of Janis CCR in the vacuum with exciting radiation. The measurements were done at 10 K of cold finger using the excitation of 577.5 nm into the $^4G_{5/2}$ level and 789 nm into $^2H_{9/2}$ + $^4F_{5/2}$ level.

Two spectra (Figure 7, curve 1 and 2) measured inside different cryostats at the same setting temperatures (T = 10 K) with laser excitation into the $^4G_{5/2}$ level ($\lambda_{ex.}$ = 577.5 nm) are remarkably different. The spectral lines of the 2 at% Nd^{3+}:LaF_3 nanoparticles mounted on the cold finger of Janis CCR are broader than they are for the same nanoparticles inside He-bath CS. This may be the evidence of higher temperature of the sample placed on the cold finger of Janis CCR. Another indicator of increased temperature is the presence of spectral lines 1' and 3' ($^4F_{3/2}(2) \rightarrow {}^4I_{9/2}$ (1) and $^4F_{3/2}(2) \rightarrow {}^4I_{9/2}(3)$) (Figure 7, curves 2, 3), which do not exist on the spectrum measured in helium vapors (Figure 7, curve 1). In the helium bath the heating of the sample by multiphonon relaxation is insignificant because helium vapors remove the heat from the sample much faster than the cold finger.

When comparing two spectra both measured inside Janis CCR, we can see that when using 789 nm excitation into $^2H_{9/2}$ + $^4F_{5/2}$ level the effect of heating is lower (Figure 7, curve 3), but still evident compared to He-bath method. This indicates that the sample does not heat so

significantly by the phonons emitted from the lower lying $^2H_{9/2}$ + $^4F_{5/2}$ mixed energy level than it is when using higher energy excitation into the $^4G_{5/2}$ level. The effect that different excitation wavelengths have different influence on the spectrum of the 2 at% Nd^{3+}:LaF_3 nanoparticles will be discussed in more details in chapter 4.4.

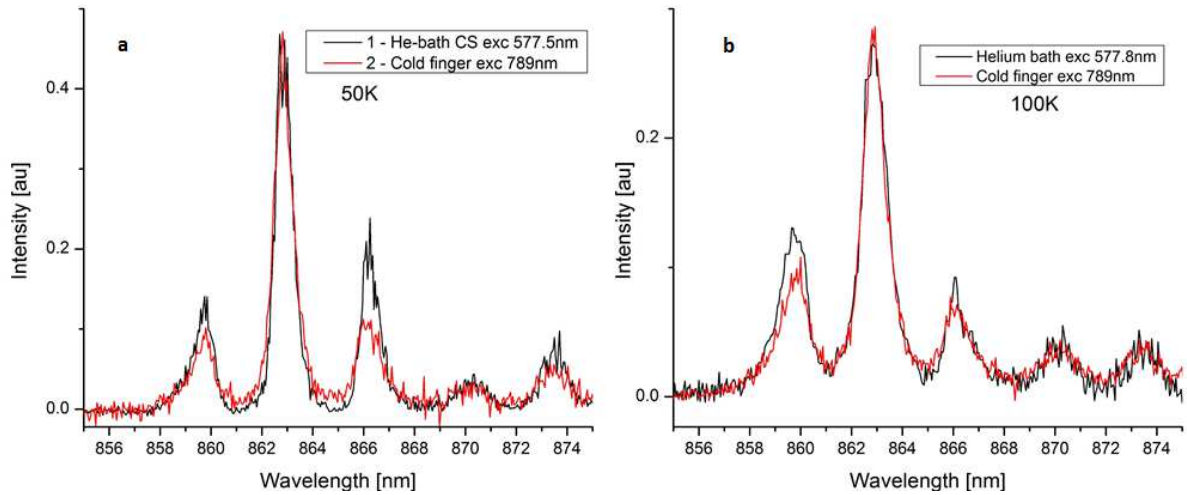

Figure 8. The fluorescence spectra of the 2 at% Nd^{3+}:LaF_3 nanoparticles, normalized to unity area. The comparison of two different cryostats at 50 K (a) and 100 K (b) temperature.

If comparing two different cryostats at 50 and 100 K temperatures (Figure 8), then we can see that the linewidths of the main peak and the intensities of peaks 1' (at 860 nm, $^4F_{3/2}(2) \rightarrow {}^4I_{9/2}(1)$) and 3' (at 870 nm, $^4F_{3/2}(2) \rightarrow {}^4I_{9/2}(3)$) are similar for two different cryostat methods. This tells us that the temperatures in two cases are roughly the same and the effect of sample heating by the phonons emitted in the nanocrystals is not significant comparing to the heating by the oven of the cryostat.

4.4 Different excitation wavelengths

To see how the excitation wavelength affect the form factor and width of the spectral lines of the 2 at% Nd^{3+}:LaF_3 nanoparticles their fluorescence spectra are measured in Janis CCR using three different excitation wavelengths at 10 K of cold finger: 522 nm (into the $^4G_{7/2}$ level), 577.5 nm (into the $^4G_{5/2}$ level), and 789 nm (into the $^2H_{9/2}$ + $^4F_{5/2}$ mixed level). Two different time gates were used. An early gate, which was set to measure the spectra just after the excitation (gate delay $t_D = 0$ and gate width $\Delta t = 5$ μs) and a late gate that measure the fluorescence spectrum starting at 200 μs after the excitation laser pulse ($t_D = 200$ μs, $\Delta t = 100$ μs).

From the spectra measured with the early gate (t_D = 0 μs, Δt = 5 μs) (Figure 9) it is seen that the different excitation wavelengths have a strong effect on the spectral shape. For 789 nm excitation wavelength into the $^2H_{9/2}$ + $^4F_{5/2}$ mixed level, which is the lowest energy level of the 2 at% Nd^{3+}:LaF_3 nanoparticles being excited in our experiment, the spectral lines (Figure 9, curve 3) responsible for transitions from $^4F_{3/2}$(1) to $^4I_{9/2}$ (1) and $^4I_{9/2}$ (2) are significantly narrower than for the other two excitation wavelengths. Also the ratio of spectral peaks 1' and 1 intensities (transitions from the second and first crystal field levels of the $^4F_{3/2}$ manifold to the $^4I_{9/2}$ (1) CF level) is visibly lower than for two other curves. This according to Eq. (7) (see below) demonstrates the lower temperature of the sample.

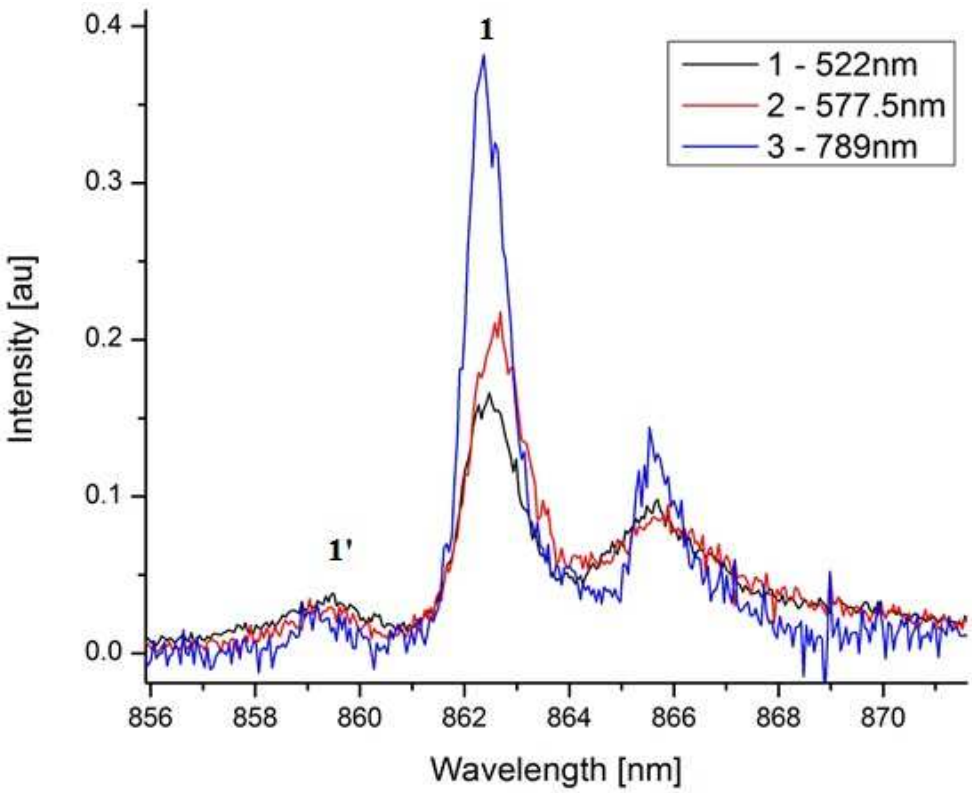

Figure 9. The fluorescence spectra of the 2 at% Nd^{3+}:LaF_3 nanoparticles at 10 K of cold finger in Janis CCR using the excitation at 522, 577.5 and 789 nm (respectively into the $^4G_{7/2}$, $^4G_{5/2}$ and $^2H_{9/2}$ + $^4F_{5/2}$ level) and the early time gate (t_D = 0 μs, Δt = 5 μs). The increase in linewidths and ratio of spectral peaks 1' and 1 intensities show that higher excitation energy will cause the temperature of the nanoparticles to be increased.

For two higher energy excitations into the $^4G_{7/2}$ and $^4G_{5/2}$ level (excitation wavelengths 522 and 577.5 nm) the difference in spectra (Figure 9, curves 2 and 3) can only be seen in the ratio of the

intensities of spectral lines 1' and 1, whereas their linewidths are almost equal. The difference in ratio shows that for the highest excitation energy the temperature of the 2 at% Nd^{3+}:LaF_3 nanoparticles is the highest.

The heating of the nanoparticles is caused by the fact that after excitation the cascade multiphonon relaxation takes place, whereby the energy is transformed to heat in form of phonons. The process of relaxation process is very fast and therefore occurs just after the excitation and before the fluorescence. The higher is the energy of excitation, the more heat is produced.

The same effects can be seen on the spectrum (Figure 10) measured with late gate (t_D = 200 μs, Δt = 100 μs). Another thing to notice is that all the spectral lines are remarkably narrower and peaks intensity ratio lower than for the early gate (Table 3).

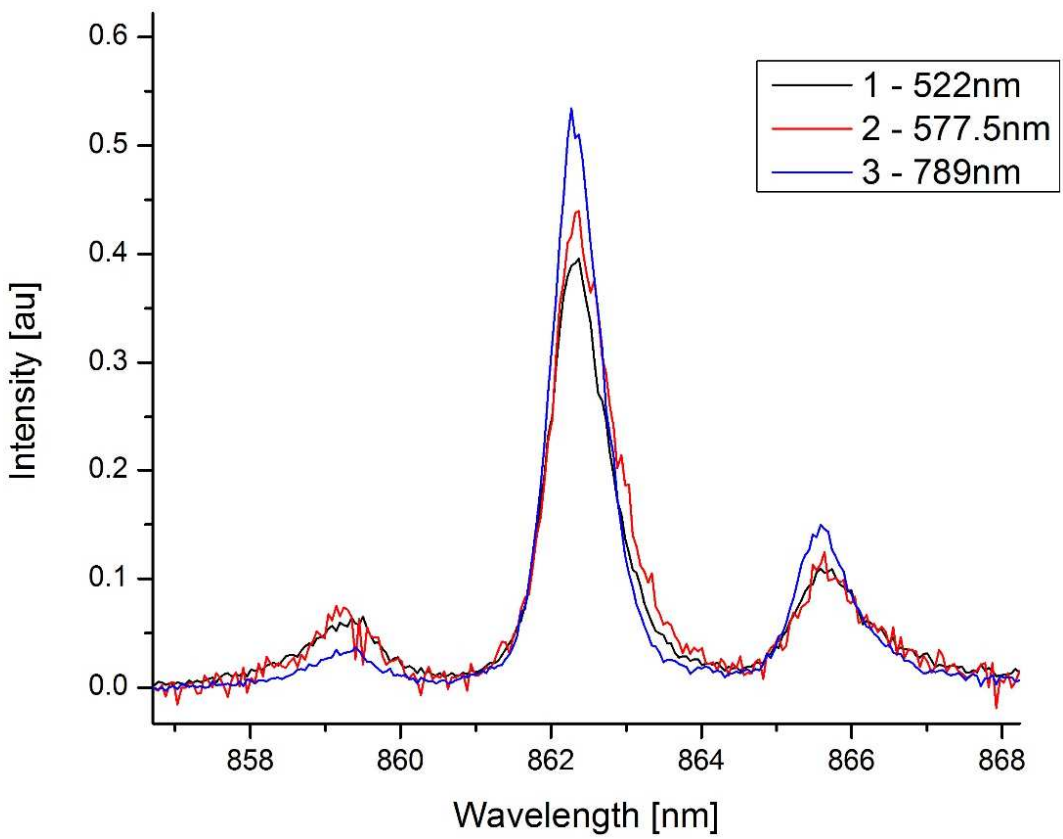

Figure 10. The fluorescence spectra of the 2 at% Nd^{3+}:LaF_3 nanoparticles at 10 K of cold finger in Janis CCR using the excitation at 522, 577.5 and 789 nm (respectively into the $^4G_{7/2}$, $^4G_{5/2}$ and $^2H_{9/2}$ + $^4F_{5/2}$ level) and the late time gate (t_D = 200 μs, Δt = 100 μs).

Table 3. The FWHM values of the main spectral line and ratio of the spectral lines intensities at 859.5 and 862.4 nm (maxima) (the $^4F_{3/2}(2) \rightarrow {}^4I_{9/2}(1)$ and $^4F_{3/2}(1) \rightarrow {}^4I_{9/2}(1)$ transitions) at different excitation wavelengths and time gate.

Excitation wavelength (nm)	FWHM (cm^{-1}) Early gate	FWHM (cm^{-1}) Late gate	Ratio Early gate	Ratio Late gate
522	18.6	12.4	0.231	0.190
577.5	17.9	12.2	0.160	0.148
789	12.6	10.4	0.088	0.070

The fact, that both the early gate and higher excitation energy cause the linewidths to be broader, is a sign of higher temperature than the setting temperature and is caused by multiphonon relaxation. A 200 μs delay makes possible to see the effect of cooling of the 2 at% Nd^{3+}:LaF_3 sample after heating by crystal lattice phonons. For the excitation by 522 nm into the $^4G_{7/2}$ level and 577.5 nm wavelength into the $^4G_{5/2}$ level it is seen (Figure 10) that the sample is less cooled than at 789 nm excitation into the $^2H_{9/2}$ + $^4F_{5/2}$ mixed level, because otherwise the FWHM of the main spectral line would be equal for both cases. It is not cooled to the same temperature as for lower energy excitation because it is heated more during the multiphonon relaxation.

If keeping in mind that larger FWHM and higher relative intensity of the 859.5 nm peak ($^4F_{3/2}(2) \rightarrow {}^4I_{9/2}(1)$) indicate higher temperature of the sample then two things become clearly visible from Table 3:

1. High energy excitations heat the sample enough to change the spectral form factor and lines widths.
2. The higher is the excitation energy the stronger is the heating
3. Using the delayed time gate it is possible to detect the cooling of the 2 at% Nd^{3+}:LaF_3 nanoparticles.

4.5 Temperature dependence

We revealed that the fluorescence spectrum of the 2 at% Nd^{3+}:LaF_3 nanoparticles has a strong dependence on temperature. To investigate this relation further we started to increase the temperature of the cold finger of Janis CCR with the heater attached to the cold finger. To have as little effect as possible from the multiphonon relaxation increasing the temperature of the sample, the excitation at 789 nm into the $^2H_{9/2}$ + $^4F_{5/2}$ mixed level was used. Again two different

time gates were used – the early gate (t_D = 0 μs, Δt = 10 μs) and the late gate (t_D = 200 μs, Δt = 100 μs). To quantify the change in the spectrum with the increasing temperature, the spectra are normalized to unity area and then the intensities of spectral lines at the $^4F_{3/2}(2) \rightarrow {}^4I_{9/2}$ (1) and $^4F_{3/2}(1) \rightarrow {}^4I_{9/2}$ (1) transitions are compared.

As the temperature rises for both the early and the late time gate the spectral peak 1', which responds to the $^4F_{3/2}(2) \rightarrow {}^4I_{9/2}$ (1) transition, intensifies as compared to the main spectral peak, which responds to the $^4F_{3/2}(1) \rightarrow {}^4I_{9/2}$ (1) transition (Figure 11). At the same time the broadening of the main spectral peak can be observed. We should have in mind the fact of the inhomogeneous broadening of the spectral lines (Figure 6).

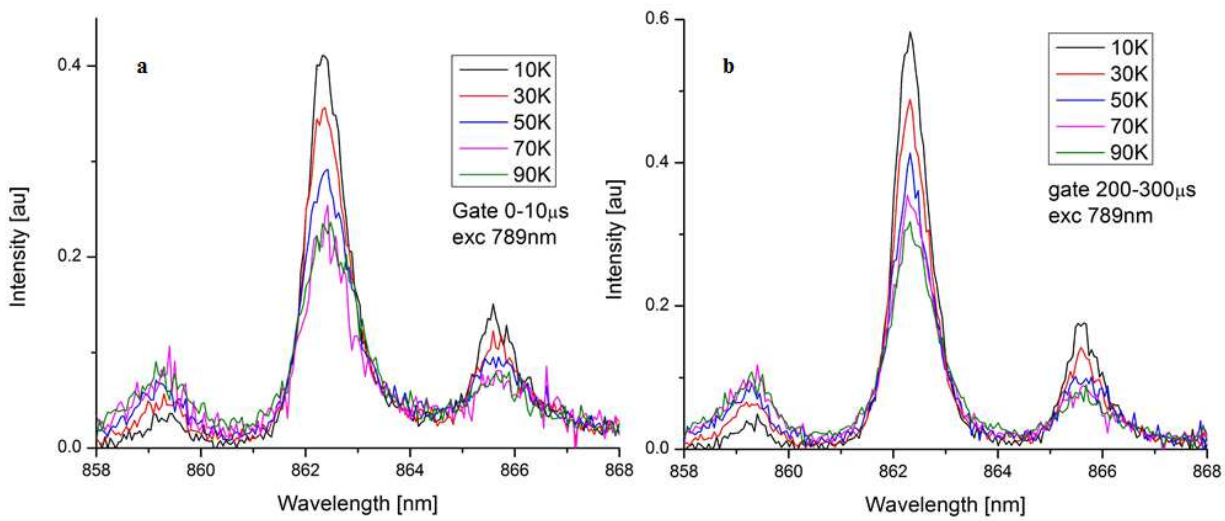

Figure 11. The fluorescence spectra of the 2 at% Nd^{3+}:LaF_3 nanoparticles at different temperature of cold finger in Janis CCR using the excitation at 789 nm into the $^2H_{9/2} + {}^4F_{5/2}$ mixed level. An early time gate (graph a, t_D = 0 μs, Δt = 10 μs) and a late time gate (graph b, t_D = 200 μs, Δt = 100 μs) were used. All graphs are normalized to unity area. This figure does not show all the temperatures that were used for measurements.

The ratio values in Table 4 show that intensity of the spectral peak 1' increases compared to the intensity of the spectral peak 1 with the temperature rise. It is visible that the values measured for spectra with late gate are mainly lower than they are for the spectra measured with early gate.

Table 4. The values of ratio of spectral peaks intensity maxima at different temperatures measured with the early (*) and the late (**) gate at 789 nm excitation into the $^2H_{9/2}$ + $^4F_{5/2}$ mixed level. 1' stands for $^4F_{3/2}(2) \rightarrow {}^4I_{9/2}$ (1) and 1 for $^4F_{3/2}(1) \rightarrow {}^4I_{9/2}$ (1) transition.

T [K]	10	20	30	40	50	60	70	80	90	100	125	150	175
$I_{1'}/I_1$ (10^{-3})*	88	114	159	209	244	267	296	328	382	406	451	455	482
$I_{1'}/I_1$ (10^{-3})**	84	104	135	207	223	254	332	339	340	379	408	443	450

The ratio between the first and the main peak could be used to determine the temperature. It is interesting to compare the experimental dependence of $I_2(T)/ I_1(T)$ obtained from the spectral measurements with the theoretically predicted.

The population of the first crystal field of the $^4F_{3/2}$ manifold according to Boltzmann distribution law is

$$n_1 = \frac{1}{1 + e^{-\frac{\Delta E}{kT}}}, \tag{1}$$

where ΔE stands for the energy difference of two crystal field levels of $^4F_{3/2}$ manifold, k is the Boltzmann constant and T the temperature of the sample. The population is connected with the intensity of the fluorescence at the $^4F_{3/2}(1) \rightarrow {}^4I_{9/2}(1)$ transition as

$$I_1 = n_1 A_1 h\nu_1 , \tag{2}$$

where A is the Einstein coefficient for spontaneous emission, h is the Planck constant and ν is the frequency of emitted photon. Considering the total population of two CF level of the $^4F_{3/2}$ manifold equal to unity we may write

$$n_1 + n_2 = 1. \tag{3}$$

From (Eq. 1) and (Eq. 2) we can get population of the second crystal field of the $^4F_{3/2}$ manifold as

$$n_2 = \frac{e^{-\frac{\Delta E}{kT}}}{1 + e^{-\frac{\Delta E}{kT}}}. \tag{4}$$

The population of that level is connected with the intensity of the fluorescence at the $^4F_{3/2}(2) \rightarrow {}^4I_{9/2}(1)$ transition as

$$I_2 = n_2 A_2 h\nu_2. \quad (5)$$

Now to get the equation for the ratio between these two transitions we divide (Eq. 5) by (Eq. 2)

$$\frac{I_2}{I_1} = \frac{n_2 A_2 h\nu_2}{n_1 A_1 h\nu_1}. \quad (6)$$

We will simplify (Eq. 6) by assuming that $A_1 \approx A_2$ and $h\nu_1 \approx h\nu_2$. The final formula becomes

$$\frac{I_2}{I_1} = \frac{n_2}{n_1} = e^{-\frac{\Delta E}{kT}}. \quad (7)$$

ΔE can easily be calculated from Table 2 by subtracting the energy of $^4F_{3/2}(1)$ level from the energy of $^4F_{3/2}(2)$ level.

$$\Delta E = (11635 - 11596)\ cm^{-1} = 39\ cm^{-1}$$

The dependence of (Eq. 7) is plotted in Figure 12 alongside with experimental dependence. We can see that the curves do not fit each other, but are similar in the regularity. For the temperatures lower than 30K the experimental dependence is lying higher than the theoretical one that indicates the higher temperature of the sample than the set temperature, whereas for the temperatures higher than 30K the situation is reversed. The later might be connected with inhomogeneous broadening and overlapping of spectral lines and requires additional study.

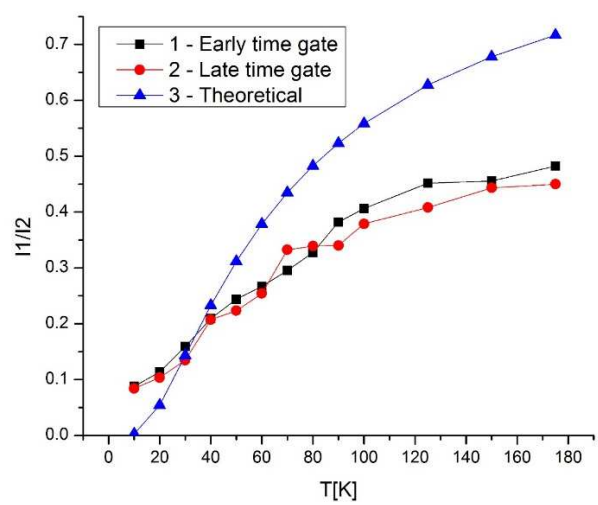

Figure 12. The dependence of the ratio of the fluorescence intensity measured at the $^4F_{3/2}(2) \rightarrow {}^4I_{9/2}$ (1) and $^4F_{3/2}(1) \rightarrow {}^4I_{9/2}$ (1) transitions on temperature of the 2 at% Nd^{3+}:LaF_3 nanoparticles. The excitation at 789 nm into the $^2H_{9/2} + {}^4F_{5/2}$ mixed level and two different time gates ($t_D = 0$ μs, $\Delta t = 10$ μs for curve 1 and $t_D = 200$ μs, $\Delta t = 100$ μs for curve 2) were used. For the theoretical dependence (curve 3) the value for ΔE was 39 cm^{-1}.

5 Summary

In the process of finding the influence of the laser excitation wavelength on the heating of the 2 at% Nd^{3+}:LaF_3 nanoparticles as the result of multiphonon relaxation some conclusions were made.

1. Six different radiative transitions ($^4F_{3/2}(2) \rightarrow {}^4I_{9/2}$ (1), $^4F_{3/2}(1) \rightarrow {}^4I_{9/2}$ (1), $^4F_{3/2}(1) \rightarrow {}^4I_{9/2}$ (2), $^4F_{3/2}(2) \rightarrow {}^4I_{9/2}$ (3), $^4F_{3/2}(1) \rightarrow {}^4I_{9/2}$ (3), $^4F_{3/2}(1) \rightarrow {}^4I_{9/2}$ (4)) were identified while measuring the fluorescence spectra of the $^4F_{3/2} \rightarrow {}^4I_{9/2}$ transition of the 2 at% Nd^{3+}:LaF_3 nanoparticles between 850 and 890 nm at low temperature. It was found that the crystal field energy level positions are the same in a bulk Nd^{3+}: LaF_3 crystal and the nanoparticles.
2. The spectral lines were found to be inhomogeneously broadened. This was determined by measuring the fluorescence kinetics at 10 K at different detection wavelengths on the most intensive spectral line (the $^4F_{3/2}(1) \rightarrow {}^4I_{9/2}$ (1) transition) and observing different time profiles of the kinetic curves.
3. When comparing fluorescence spectra excited by tunable laser of the 2 at% Nd^{3+}:LaF_3 nanoparticles inside the Janis CCR, for which different cooling methods were used (He-bath and CCR), we found a well detectable heating due to the multiphonon relaxation of the optical excitation. The effect of heating of the nanoparticles was determined qualitatively from the intensity ratio of the fluorescence spectral lines connected with two optical transitions from two Stark levels of the $^4F_{3/2}$ manifold to the ground crystal field level of the $^4I_{9/2}$ manifold. This brought the expectation that exciting the Nd^{3+} ions into different energy levels will heat the particles to different extents. This hypothesis was confirmed by using different excitation wavelengths. The excitation into higher lying energy levels heats the sample enough to change the spectral form factor and lines widths. The expected relation between excitation wavelength and the amount of heating was also confirmed. The higher is the energy of the excited level the stronger is the heating caused by multiphonon relaxation.

Summing up, besides possible application for bioimaging the Nd^{3+}:LaF_3 nanoparticles are a good candidate for photo-induced heating for hyperthermia of cancer tumors. I think that Nd^{3+}:LaF_3 nanoparticles should be studied further.

6 Acknowledgements

I would like to thank my supervisor Yury Orlovskiy for setting the problem and experiments, as well as his patience and calmness, when it was necessary to explain something more than once or twice to me, and Laurits Puust for helping me with the measurements. I am also grateful to Kerda Keevend for synthesizing the nanoparticles and for giving advice on writing this work. The final thanks go to all the members of LLS of Institute of Physics for friendly and helpful atmosphere.

7 Laserergastuse lainepikkuse mõju neodüümiga dopeeritud fluoriidi nanoosakeste soojendamisele multifoononilise relaksatsiooni tulemusena

Kaarel Kaldvee

Kokkuvõte

Haruldaste muldmetalli ioonidega dopeeritud nanoosakeste sobivus vähiraviks on järjest rohkem uuritud. Neodüümiga dopeeritud LaF_3 nanokristalle peetakse juba headeks kandidaatideks vähirakkude kiirguslikul tuvastamisel. Selles töös uuritakse antud osakeste soojenemist mitmefoononilise relaksatsioonil optilise ergastuse tõttu, mille potentsiaalne rakendus on vähirakkude hävitamine hüpertermiaga.

Selle jaoks sünteesiti 2 at% Nd^{3+}:LaF_3 nanoosakesed ja uuriti nende fluorestsentskiirgust. Uuritava objekti jahutamiseks 10 Kelvinini kasutati kahte erinevat tüüpi krüostaate: heeliumi aurudega jahutamist ja suletud tsükliga krüostaati, millel objekt on vaakumis külmsõrmel. $^4F_{3/2} \rightarrow {}^4I_{9/2}$ ülemineku kiirgusspektrit mõõdeti vahemikus 850 kuni 890 nm kolme erineva lainepikkusega laserimpulsside ergastusel: 522, 577.5 ja 789 nm (vastavalt $^4G_{7/2}$, $^4G_{5/2}$ ja $^2H_{9/2}$ + $^4F_{5/2}$ energianivoodele). Lisaks kasutati fluorestsents-spektrite mõõtmisel kahte erinevat ajaakent: kohe pärast ergastust (5 μs laiune) ja 200 μs pärast ergastust (100 μs laiune).

Selle töö käigus määrati uuritavas lainepikkuste vahemikus esinevale kuuele spektraaljoonele vastavad üleminekud ($^4F_{3/2}(2) \rightarrow {}^4I_{9/2}$ (1), $^4F_{3/2}(1) \rightarrow {}^4I_{9/2}$ (1), $^4F_{3/2}(1) \rightarrow {}^4I_{9/2}$ (2), $^4F_{3/2}(2) \rightarrow {}^4I_{9/2}$ (3), $^4F_{3/2}(1) \rightarrow {}^4I_{9/2}$ (3), $^4F_{3/2}(1) \rightarrow {}^4I_{9/2}$ (4)). Leiti, et Starki energiatasemete asukohad on samad Nd^{3+}: LaF_3 kristalli ja nanokristallide jaoks. Mõõtes fluorestsentsi kineetikaid kõige intensiivsemal spektri joonel ($^4F_{3/2}(1) \rightarrow {}^4I_{9/2}$ (1) üleminek) erinevatel lainepikkustel tuvastati spektri mittehomogeenne laienemine.

Erinevatel seadistustel kiirgusspektrite omavahelisel võrdlemisel avastati hästi tuvastatav Nd^{3+}:LaF_3 nanoosakeste soojenemine multifoononilise relaksatsiooni tõttu optilisel ergastusel. Kinnitati seos ergastamiseks kasutatava kiirgusenergia ja soojendamise ulatuse vahel.

Jättes kõrvale Nd^{3+}:LaF_3 nanoosakeste võimalik rakendamine vähkkasvajate avastamiseks kehas, võib järeldada, et uuritud osakested on sobivad kasutamiseks vähiravis fotoindutseeritud hüpertermia kujul ja neid tuleks uurida edasi.

8 References

[1] World Health Organization, "Cancer fact sheet," Feb 2015. [Online]. Available: http://www.who.int/mediacentre/factsheets/fs297/en/. [Accessed 22.05.2015].

[2] Yurii V. Orlovskii, Alexander S. Vanetsev, Anastasiya V. Ryabova, Konstantin K. Pukhov, Alexander V. Popov, Elena V. Samsonova, Kerda Keevend, Igor D. Romanishkin, Ilmo Sildos and Victor B. Loschenov, "Nanoscaled Rare-Earth Doped Crystal Heater," in *Frontiers in Optics 2014*, Tucson, Arizona, USA, July 2014; Yurii V. Orlovskii, Alexander S. Vanetsev, Igor D. Romanishkin, Anastasiya V. Ryabova, Konstantin K. Pukhov, Alexander E. Baranchikov, Elena V. Samsonova, Kerda Keevend, Ilmo Sildos and Victor B. Loschenov, "Laser heating of the $Y_{1-x}Dy_xPO_4$ nanocrystals," *Optical Materials Express,* vol. 5, no. 5, pp. 1230 - 1239 (2015).

[3] Elena V. Samsonova, Alexander V. Popov, Alexander S. Vanetsev, Kerda Keevend, Elena O. Orlovskaya, Valter Kiisk, Sven Lange, Urmas Joost, Kaarel Kaldvee, Uno Mäeorg, Nikolay A. Glushkov, Anastasiya V. Ryabova, Ilmo Sildos, Vyacheslav V. Osiko, Rudolf Steiner, Victor B. Loschenov and Yurii V. Orlovskii, "An energy transfer kinetic probe for OH-quenchers in the Nd^{3+}:YPO_4 nanocrystals suitable for imaging in the biological tissue transparency window," *Phys.Chem.Chem.Phys.,* vol. 16, pp. 26806-26815 (2014).

[4] H. H. Caspers, H. Rast and R. Buchanan, "Intermediate Coupling Energy Levels for $Nd^{3+}(4f^3)$ in LaF_3," *The Journal of Chemical Physics,* vol. 42, no. 9, pp. 3214-3217 (1965).

[5] O. Alimov, T. Basiev and S. Mirov, "Spectral and relaxation characteristics of local electron states of impurities in structurally disordered matrices," *Proceedings of the Institue of General Physics,* vol. 9, pp. 1-65 (1990).

[6] M. Sauer, J. Hofkens and J. Enderlein, "Basic Principles of Fluorescence Spectroscopy," in *Handbook of Fluorescence Spectroscopy and Imaging*, Weinheim, Wiley-VCH (2011).

[7] D. Jaque, L. Martinez Maestro, B. del Rosal, P. Haro-Gonzalez, A. Benayas, J. Plaza, E. Martin Rodriguez and J. Garcia Sole, "Nanoparticles for photothermal therapies," *Nanoscale,* vol. 6, no. 16, pp. 9494-9530 (2014).

[8] Elena V. Samsonova, Alexander V. Popov, Alexander S. Vanetsev, Kerda Keevend, Kaarel Kaldvee, Laurits Puust, Alexander E. Baranchikov, Anastasiya V. Ryabova, S. Fedorenko, Valter Kiisk, Ilmo Sildos, Jaak Kikas, Rudolf Steiner, Victor B. Loschenov and Yurii V. Orlovskii, "Fluorescence quenching mechanism for water-dispersible Nd^{3+}:KYF_4," *Journal of Luminescence,* vol. Article in press (2015).

[9] E. Rocha, K. Upendra Kumar, C. Jacinto, I. Villa, F. Sanz-Rodriguez, M. Iglesias de la Cruz, A. Juarranz, E. Carrasco, F. van Veggel, E. Bovero, J. Garcia Sole and D. Jaque, "Neodymium-Doped LaF_3 Nanoparticles for Fluorescence Bioimaging in the Second Biological Window," *Small,* vol. 6, no. 10, pp. 1141-1154 (2014).

Non-exclusive licence to reproduce thesis and make thesis public

I, _____Kaarel Kaldvee_____,

(author's name)

herewith grant the University of Tartu a free permit (non-exclusive licence) to:

reproduce, for the purpose of preservation and making available to the public, including for addition to the DSpace digital archives until expiry of the term of validity of the copyright, and

make available to the public via the university's web environment, including via the DSpace digital archives, as of **1.06.2017** until expiry of the term of validity of the copyright,

THE INFLUENCE OF LASER EXCITATION WAVELENGTH ON THE HEATING OF THE NEODYMIUM DOPED FLUORIDE NANOPARTICLES AS THE RESULT OF THE MULTIPHONON RELAXATION,

(title of thesis)

supervised by _____ Dr. hab., Ph.D. Yury Orlovskiy _____,

(supervisor's name)

I am aware of the fact that the author retains these rights.

This is to certify that granting the non-exclusive licence does not infringe the intellectual property rights or rights arising from the Personal Data Protection Act.

Tartu, **26.05.2015**